Chemical Science

RSC Publishing

EDGE ARTICLE

View Article Online
View Journal | View Issue

Cite this: *Chem. Sci.*, 2013, **4**, 2858

Photophysical pore control in an azobenzene-containing metal–organic framework†

Jonathan W. Brown,‡*[a] Bryana L. Henderson,‡[b] Matthew D. Kiesz,[b] Adam C. Whalley,[c] William Morris,[a] Sergio Grunder,[c] Hexiang Deng,[a] Hiroyasu Furukawa,[a] Jeffrey I. Zink,[b] J. Fraser Stoddart[c] and Omar M. Yaghi*[adef]

Received 3rd October 2012
Accepted 19th April 2013

DOI: 10.1039/c3sc21659d

www.rsc.org/chemicalscience

The synthesis and structure of an azobenzene functionalized isoreticular metal–organic framework (azo-IRMOF-74-III) [$Mg_2(C_{26}H_{16}O_6N_2)$] are described and the ability to controllably release a guest from its pores in response to an external stimulus has been demonstrated. Azo-IRMOF-74-III is an isoreticular expansion of MOF-74 with an etb topology and a 1-D hexagonal pore structure. The structure of azo-IRMOF-74-III is analogous to that of MOF-74, as demonstrated by powder X-ray diffraction, with a surface area of 2410 $m^2\ g^{-1}$ BET. Each organic unit within azo-IRMOF-74-III is decorated with a photoswitchable azobenzene unit, which can be toggled between its *cis* and *trans* conformation by excitation at 408 nm. When propidium iodide dye was loaded into the MOF, spectroscopic studies showed that no release of the luminescent dye was observed under ambient conditions. Upon irradiation of the MOF at 408 nm, however, the rapid wagging motion inherent to the repetitive isomerization of the azobenzene functionality triggered the release of the dye from the pores. This light-induced release of cargo can be modulated between an on and an off state by controlling the conformation of the azobenzene with the appropriate wavelength of light. This report highlights the ability to capture and release small molecules and demonstrates the utility of self-contained photoactive switches located inside highly porous MOFs.

Introduction

Metal–organic frameworks (MOFs), are extended crystalline structures containing metal oxide units bridged by organic linkers. They are highly porous and typically exhibit large surface areas. A wide variety of organic linkers have been incorporated into MOFs, highlighting the isoreticular principle whereby the organic linkers can be changed, yet analogous structural types can be synthesized.[1–4] Variation of the functional groups present in MOFs have led to applications in chemical sensing,[5,6] gas separation,[7] gas storage,[8,9] catalysis,[10] and drug delivery.[11] Despite the large library of MOFs reported in the literature, to date the storage and release of guest molecules has relied[12] solely on the uncontrolled diffusion of cargo into and out of the extended structures of the MOFs. Although many MOFs have been synthesized, none have demonstrated on-command release of stored guest molecules using a controllable external stimulus.

One such functionality, which demonstrated promise for the controlled release of cargo from the pores of a MOF, is the azobenzene unit. Azobenzene provides a source of reversible and photo-controllable *cis*/*trans* isomerizations.[13–15] This conformational switching results in significant changes in the length of the molecule (9 Å in the *trans* form to 5.5 Å in the *cis* form)[16] and, as a result, this photoswitchable system has been incorporated into a variety of rigid materials including films and nano-structures.[17–30] Furthermore, the integration of azobenzene units has been employed recently in the one-dimensional (1-D) pores of mesoporous silica nanoparticles where it was demonstrated[31,32] that the on-command release of cargo molecules from the pores is possible. Photoactive linkers have been incorporated into MOFs and shown interesting adsorption and storage properties that have been directly linked to the photoactivity of those frameworks.[33–37] Recently two MOFs were synthesized[38,39] containing azobenzene units, however, the

[a]*Center for Reticular Chemistry, Center for Global Mentoring, Department of Chemistry and Biochemistry, University of California, Los Angeles, California 90095, USA. E-mail: jbrown@chem.ucla.edu*

[b]*Department of Chemistry and Biochemistry, University of California, Los Angeles, 607 Charles E. Young Drive East, Los Angeles, California 90095-1569, USA*

[c]*Center for the Chemistry of Integrated Systems and Department of Chemistry, Northwestern University, 2145 Sheridan Road, Evanston, Illinois 60208, USA*

[d]*Department of Chemistry, University of California, Berkeley, California, 94720, USA. E-mail: yaghi@berkeley.edu*

[e]*Molecular Foundry, Division of Materials Sciences, Lawrence Berkeley National Laboratory, Berkeley, California, 94720, USA*

[f]*NanoCentury KAIST Institute, Graduate School of EEWS (WCU), Korea*

† Electronic supplementary information (ESI) available: Full synthetic and analytic details are available in the supplementary information. See DOI: 10.1039/c3sc21659d

‡ These authors contributed equally.

nature of the pores in these MOFs produced steric restrictions that limited photoswitching applications. We chose to incorporate the photoswitch into a MOF-74 based structure, to combat these steric limitations. Due to a unique binding motif inherent to MOF-74, the inorganic clusters and organic struts form linear stacks producing large, non-interpenetrated 1-D hexagonal pores. This unique architecture will force the azobenzene units directly into the channels where the isomerization of each unit will have a direct impact on the aperture size of a single 1-D channel. Therefore, the photodynamic switching of azobenzene combined with the 1-D structure of this MOF has the potential to allow for controlled cargo delivery from a MOF.

Here, we report the synthesis and photoisomerization studies of a non-interpenetrated azobenzene-derivatized MOF, azo-IRMOF-74-III, which contains 1-D pores. In this particular MOF, the size and shape of the apertures are controlled by the conformational changes in the azobenzenes, which can be reversibly switched from *trans* to *cis* or *cis* to *trans* using UV or visible irradiation, respectively. When all of the azobenzene units are in the *trans* conformation the pore apertures are 8.3 Å in diameter, but upon switching to the *cis* conformation the size of the aperture is increased significantly (10.3 Å).

This photodynamic MOF exhibits improved photoswitching over previously synthesized azobenzene-derivatized structures because the azobenzenes are evenly spaced within the crystalline framework. The photophysical properties of the MOF have been investigated by ^{1}H NMR and UV-Vis spectroscopy, and information obtained from these techniques has been used to choose a wavelength of light capable of isomerizing the azobenzene units back and forth between their two possible conformations. Spectroscopic monitoring of the release of a fluorescent guest molecule reveals that the dye remains contained in the MOF until irradiation at an appropriate wavelength. This successful containment and on-command release demonstrates the utility of self-contained photo-active switches in highly porous MOFs.

Experimental detail

Synthesis of azo-IRMOF-74-III

The synthesis of the azobenzene-functionalized linkers involves (Scheme 1) a palladium-catalyzed *Suzuki–Miyaura* cross-coupling reaction between 2,5-dibromonitrobenzene and the phenylboronic ester **1** in a degassed 1,4-dioxane–H_2O mixture employing $PdCl_2$(dppf) as the catalyst and CsF as the base to yield the nitro derivative **2**. Treatment of 2 with RANEY® Ni and H_2 gas in EtOAc at 50 °C, serves to facilitate both the removal of the benzyl protecting groups and reduce the nitro group to produce the aniline derivative **3** in nearly quantitative yield. Subjecting **3** to excess of nitrosobenzene in acetic acid at 80 °C yielded the azobenzene **4**, which could be converted to the dicarboxylic acid **5**, by saponification of the methyl esters.

Azo-IRMOF-74-III was synthesized by combining $Mg(NO_3)_2 \cdot 6H_2O$ (80 mg, 0.315 mmol) and the azobenzene-functionalized linker (42.5 mg, 0.09 mmol) in a solution of *N*,*N*-dimethylformamide (DMF) (7.5 mL), EtOH (0.5 mL) and H_2O (0.5 mL) for 24 h at 120 °C. After 24 h, the red crystals were collected by filtration.

Characterization of azo-IRMOF-74-III

Powder X-ray diffraction was used for structural determination as the microcrystalline material produced from the MOF synthesis did not diffract sufficiently for single crystal elucidation. Since a higher level of characterization is achieved by producing a solvent and guest free framework, the crystals were sequentially washed with DMF (3 × 10 mL) and methanol (3 × 10 mL) and then evacuated on a supercritical CO_2 dryer over the course of 12 hours. Following this activation process, thermal

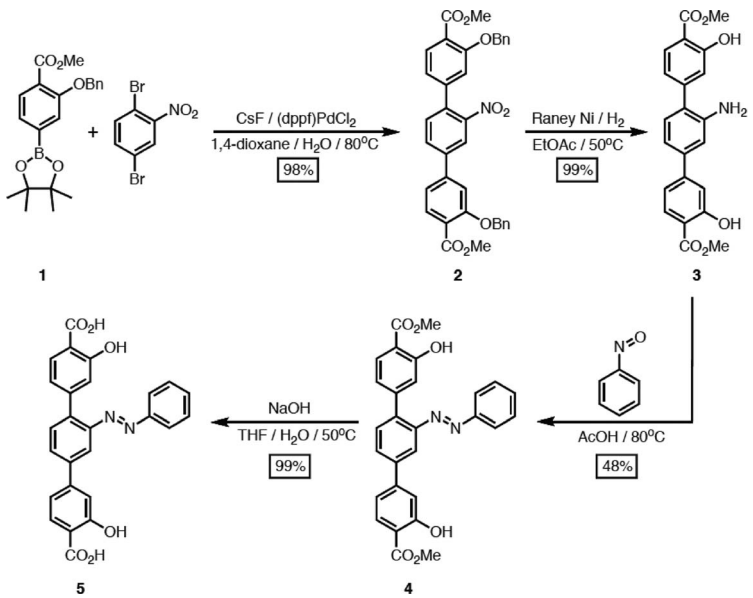

Scheme 1 Synthesis of azobenzene-functionalized MOF struts.

gravimetric analysis (TGA) was used to confirm that all of the solvent had been removed from the pores of the framework; *i.e.*, there was no significant weight loss up to 275 °C (Fig. S-4†).

Azo-IRMOF-74-III is an isoreticular expansion of MOF-74, in which helical Mg–O–C rods are constructed from hexacoordinate Mg(II) centers. The rods are connected *via* azobenzene functionalized terphenylene unit **5** to produce one-dimensional pores, which have a diameter of 19.5 Å. This structure was simulated using the Forcite module of Materials Studio and was confirmed with the Rietveld method. Because the one-dimensional pores in azo-IRMOF-74-III are lined with azobenzene groups that project toward the middle of the pore, the size and shape of the pore aperture directly depend on the *cis* or *trans* configuration. With all azobenzene functionalities in the *trans* configuration the idealized pore aperture is 8.3 Å, but if all functionalities are *cis*, the aperture is larger 10.3 Å (Fig. 1). The PXRD pattern for azo-IRMOF-74-III was indexed on a trigonal unit cell and refined using the Rietveld method in the Reflex module of Materials Studio, yielding cell parameters

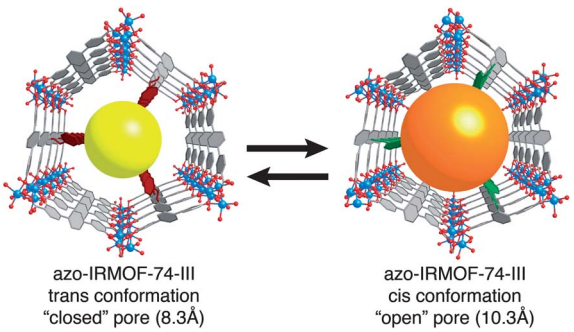

Fig. 1 Viewing idealized azo-IRMOF-74-III down the c-axis displays one-dimensional pores and azobenzene functional groups projecting into the pores. The yellow and orange balls represent pore aperture in idealized azo-IRMOF-74-III, when the azobenzene functional groups are in *trans* and *cis* conformation, respectively.

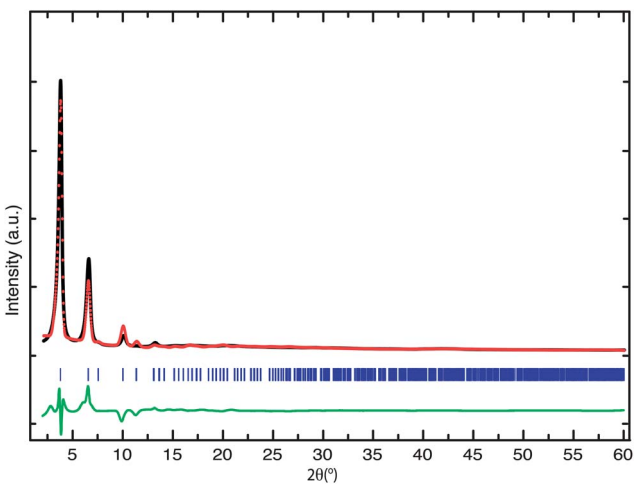

Fig. 2 Indexed experimental (red) and refined (black) PXRD patterns of azo-IRMOF-74-III after Rietveld refinement. The difference plot is indicated in green. Blue ticks indicate the positions of Bragg reflections.

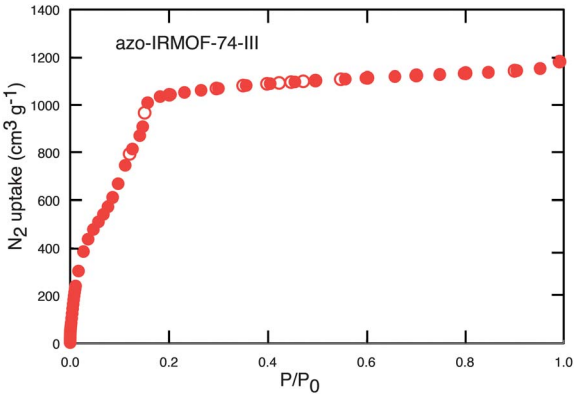

Fig. 3 Nitrogen isotherm of azo-IRMOF-74-III carried out on activated sample at 77 K. Adsorption and desorption branches are represented by solid and open circles respectively. A surface area of 2410 $m^2\ g^{-1}$ was calculated from Brunauer–Emmett–Teller (BET) analysis.

$a = 46.771(26)$ Å, $b = 46.771(26)$ Å and $c = 6.869(83)$ Å (residuals: Rp = 12.08%, Rwp = 17.68%) (Fig. 2).

Azo-IRMOF-74-III was further characterized by cross-polarization magic-angle spinning (CP/MAS) ^{13}C NMR spectra (Fig. S-5†). From experiments on the activated material, the expected resonances at 174 ppm for the carbonyl carbon atoms and 166 and 114 ppm for the aromatic carbon atoms of incorporated **5** were found. No free **5** was observed in the MOF spectra, confirmed by a lack of peaks at 176, 160, and 108 ppm.

To confirm the porosity of azo-IRMOF-74-III, N_2 isotherms at 77 K were measured on activated samples. From the Brunauer–Emmett–Teller (BET) analysis a surface area of 2410 $m^2\ g^{-1}$ was calculated (Fig. 3). To date, this is the highest recorded surface area of a MOF containing photoswitchable units.

Results and discussion

Photophysics of the azobenzene linker

The azobenzene functionalized linker used to synthesize azo-IRMOF-74-III exhibits the expected isomerization when exposed to UV and visible light. While previous studies of azobenzene and its derivatives have examined the photophysical properties in solution and various molecular environments, incorporation to a new platform warrants investigation of its photochromic properties. The UV-vis absorption experiments discussed in this section will thus demonstrate the performance of the azobenzene moiety within the rigid confines of a MOF.

The UV-vis absorption spectrum of non-irradiated **5** exhibits two prominent peaks, close in energy, in the near UV (Fig. 4a). Irradiation of **5** with UV light (which typically induces a *trans*-to-*cis* isomerization for azobenzene) results in dramatic changes in the absorption spectrum; *i.e.* the emergence of a new absorption band in the visible region. Although the photoisomerization process is evident, transitions due to the terphenyl moiety overshadow those of the azobenzene functional group in both the pre- and post-irradiation absorption spectra. In addition, the fact that the absorption spectra of the photostationary states are not necessarily purely those of the *trans* or

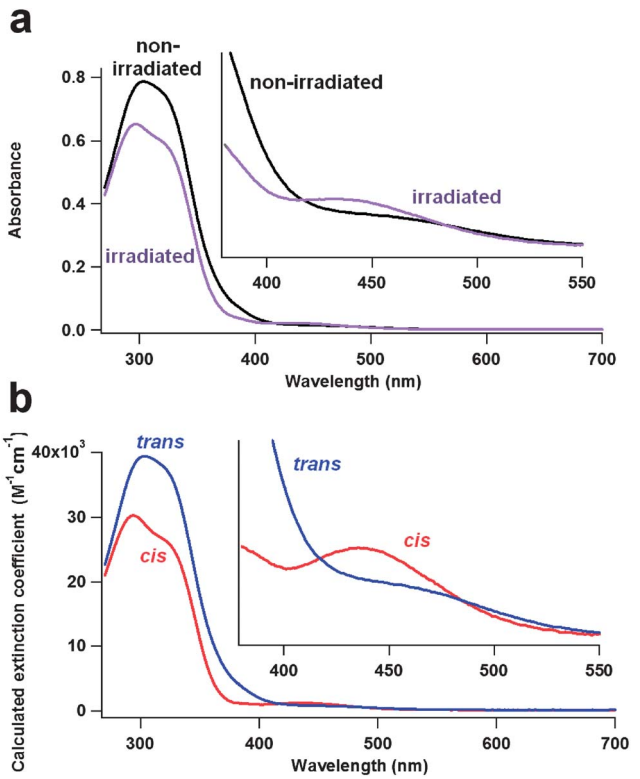

Fig. 4 Pre-(black trace) and post-(cyan trace) irradiation UV-vis absorption spectra of **5** (a) and *cis* (red trace) and *trans* (blue trace) spectra calculated from eqn (1) using relative *cis* and *trans* peak integrations from ^{1}H NMR spectra (b). Spectra for (a) (20 M in DMSO) were irradiated with 15 mW of light from a 377 nm diode laser for 30 minutes.

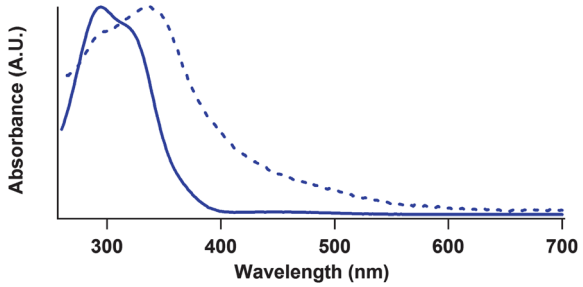

Fig. 5 Comparison of absorption spectra of **5** (solid trace) with the absorption spectrum of azo-IRMOF-74-III (dotted trace). The transition seen at ~315 nm shifts to 337 nm upon coordination of the linker with the magnesium atoms is attributed to a π–π* transition involving the C=O functionalities on the outer rings.

cis isomers, respectively, further complicates analysis. Correlation of absorption spectra with ^{1}H-NMR data elucidated spectral assignments and will be discussed in more detail below.

Relative concentration ratios of the isomers were determined with ^{1}H NMR (ESI†) and combined with UV-vis spectroscopy to calculate pure *cis* and *trans* spectra. Examination of the NMR data for a pre-irradiated solution of azobenzene in DMSO (5 mM for NMR experiments, but diluted to 20 μM for absorption spectra) stored in the dark at room temperature demonstrated the absence of the *cis* isomer. In contrast, the NMR spectrum of the photostationary state achieved after 30 minutes of irradiation with near-UV light (377 nm, 15 mW) contained peaks from both the *cis* and *trans* isomers. Integration of the *cis* and *trans* peaks in the irradiated solution yielded a *trans*/*cis* ratio of 0.43 (70% of *trans*-azobenzenes had converted to the *cis* configuration). Pre- and post-irradiation absorption data were correlated with the relative isomer concentrations to calculate a pure *cis* absorption spectrum according to the following equation:

$$\varepsilon_c = \frac{\frac{1}{cl}\left[A_2\left(\frac{1}{r_2}+1\right) - A_1\left(\frac{1}{r_1}+1\right)\right]}{\frac{1}{r_2}-\frac{1}{r_1}} \quad (1)$$

where ε_c is the calculated *cis* extinction coefficient (M^{-1} cm^{-1}), c is the concentration of **5** (M), l is the path-length of the cuvette (cm), A_1 and A_2 are the pre- and post-irradiation absorbances, respectively, and r_1 and r_2 are the pre- and post-irradiation *trans*/*cis* isomer ratios, respectively. The resulting pure *cis* and *trans* spectra (Fig. 4b) reveal a clearer representation of the transitions of **5**. While each of the calculated *cis* and *trans* spectra contain appreciable absorption in the UV region due to the inherent absorption from the ter-phenylene structure, the *trans* isomer absorbs more than the *cis* isomer in the UV and the *cis* isomer absorbs more than the *trans* in the visible region as expected.

The UV and visible absorption peaks of the azo-benzene moiety are assigned to π–π* and n–π* electronic transitions, respectively. Both *cis* and *trans* calculated spectra contain a peak near 300 nm with a shoulder at 315 nm, which are attributed to the common ter-phenylene moiety. The higher energy transition near 300 nm is assigned to a π–π* transition that does not shift when the linker is coordinated to the metal atoms in the MOF. However, the shoulder at 315 nm, which is assigned to a π–π* transition involving the C=O functionalities on the outer rings, shifts to 337 nm upon coordination within the MOF structure (Fig. 5). In the calculated spectrum of the *trans* isomer, a shoulder near 365 nm is attributed to an azobenzene π–π* transition. A weaker n–π* azobenzene transition is found at 438 nm in the calculated *cis* spectrum.

To characterize the photoproperties of linker **5** used in this MOF, absorption spectra were obtained as a function of irradiation time with UV and blue light. A 50 μM solution of **5** was exposed to 15 mW of 377 nm excitation with continuous stirring; its absorption spectra upon irradiation are plotted in Fig. 6. Irradiation of **5** in the near UV (377 nm, Fig. 6a) leads to excitation of the azobenzene π–π* transition seen in the calculated *trans* spectrum.

Since the *cis* isomer has no appreciable absorbance in the near-UV, the probability of *trans* to *cis* isomerization is higher than *cis* to *trans* isomerization and thus the population of the *cis* species increases. Additionally, competing absorption from the terphenylene portion of the linker is relatively low at 377 nm, so the incident photons are able to reach the azobenzene more efficiently. To convert the molecule back to the *trans* species, the azobenzene linkers were irradiated in the visible region (457 nm, Fig. 6b) where the absorbance of the *cis* isomer is higher than the absorbance of the *trans* isomer. The absorption spectra show an increase in the n–π* band at 438 nm and a

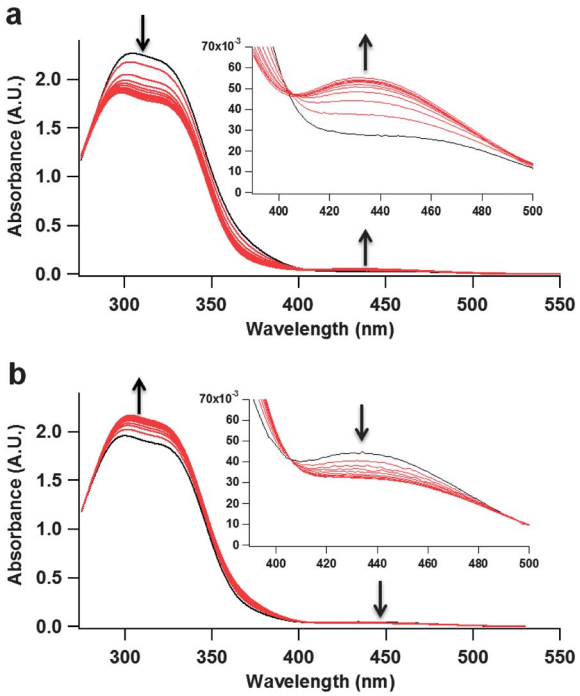

Fig. 6 Change in absorbance of the azobenzene linker with (a) 377 nm irradiation followed by (b) 457 nm irradiation. Each trace represents 15 seconds of irradiation. The first trace is plotted in black for clarity.

decrease in the 300 nm peaks upon near-UV irradiation and the opposite trend with visible irradiation, indicating reversible isomer population changes without decomposition of the linker.

The *cis* and *trans* isomers of the linker have an isosbestic point at 402 nm that does not shift when coordinated to magnesium (Fig. S-8†). Excitation wavelengths in this region can be utilized for stimulating repetitive large amplitude motions. These large amplitude motions have been used to activate the release of cargo from porous substances,[40,41] and *cis–trans* isomerization expels cargo in a similar way to the MOFs in this study.

Trapping and release of cargo on command

To test the ability of azo-IRMOF-74-III to store and release cargo, a luminescent dye (propidium iodide, Sigma) was loaded into the hexagonal channels so that the release due to photoisomerization could be observed spectroscopically. This dye was specifically chosen because its size, 8 × 11 × 16 Å without counterion, matches well with the pore aperture of azo-IRMOF-74-III, between 8.3 and 10.3 Å depending on conformation of azobenzene linker (Fig. S-1 and S-2†). When comparing pore diameter to the dye, it can be seen that the dye cannot easily diffuse into the MOF unless the azobenzene functionalities are in the *cis* conformation (Fig. S-3†). To load the azo-MOFs, 100 mg of particles were stirred in a 1 mM ethanolic solution of propidium iodide for 3 days under exposure to room lights. The loading process is driven by a concentration gradient and the photoisomerization afforded by room lights. UV-vis spectra of a propidium iodide solution acquired before and after loading demonstrate a loading capacity of 0.4 wt% (Fig. S-7†). While minimizing light exposure the particles were washed thoroughly with ethanol to remove surface adsorbed dye. Subsequently the sample was placed in the corner of a 2 cm × 1 cm fluorimetric cuvette. A stir bar was placed in the opposite corner to facilitate mixing of the solution, and the cuvette was filled with spectroscopic-grade ethanol. The solution in the cuvette was stirred carefully to avoid disturbing the azo-IRMOF-74-III particles yet facilitate the diffusion of the dye. A probe beam (30 mW, 568 nm) was used to excite the propidium dye in the ethanol solution above the particles, and its fluorescence intensity was integrated and plotted as a function of time (Fig. 7a).

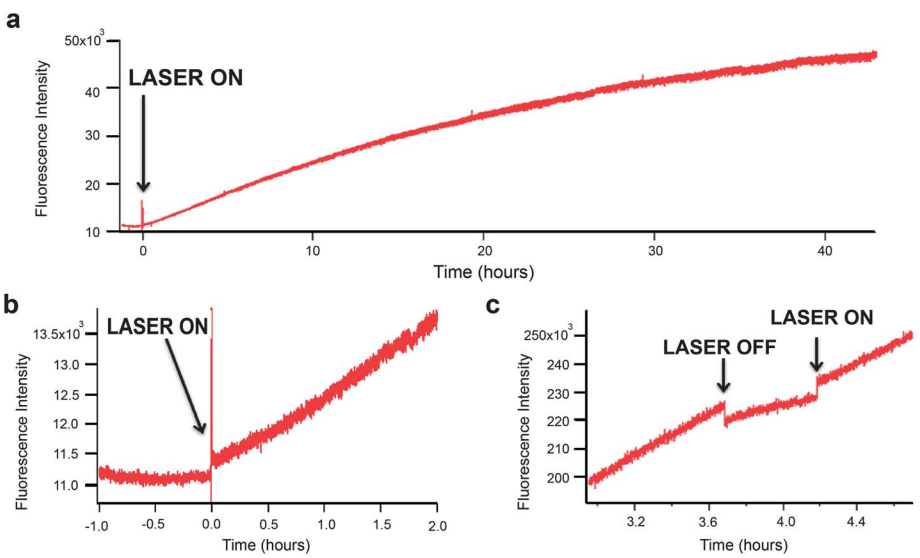

Fig. 7 (a) Typical release of propidium dye from azo-IRMOF-74-III as a function of time, (b) detailed view of the baseline and start of laser irradiation (marked by the sharp line), and (c) an on/off trial, where the excitation beam was temporarily removed mid-release. The dye continues to diffuse away from the MOF, but the rate of release is drastically reduced.

As seen in Fig. 7b, there is no increase in propidium iodide intensity prior to laser activation of the *cis*/*trans* isomerization motions in the azo-IRMOF-74-III particles. This indicates that the azobenzene-functionalized MOF acts as an excellent container, and that no dye escapes from the MOF channels until an external light source of the proper wavelength is added.

After a baseline was established with the probe beam, a 50 mW pump beam at 408 nm (wavelength near the isosbestic point) activated the *cis–trans* wagging motions and expelled the dye from the MOF channels. A clear release was observed which began to level off after 40 hours (see Fig. 7a). This release took much longer than in azobenzene-derivatized MCM-41 nanoparticles, which can possibly be attributed to the fact that the MOF structure's pores are longer and narrower.[42] Additionally, the physical interactions between the guest molecules and the host metal–organic framework may be vastly different than those seen in MCM-41. To demonstrate the necessity of the pump beam near the isosbestic point of the azobenzene moiety, a 647 nm laser was employed as a pump beam in a subsequent experiment (Fig. S-6†). No release was observed until the 647 nm laser was replaced with one near the isosbestic point. The release seen in Fig. 7a can also be controlled by increasing or decreasing the incident power or removing the beam entirely; blockage of the 408 nm pump beam caused the release to slow down (see Fig. 7c), but upon reintroduction of the beam the original release rate resumed. The sharp increases and decreases seen in the fluorescence spectra of Fig. 7 when the laser is turned on and off, respectively, are due to effects from laser scattering. When the laser impinges upon the MOF particles, the uneven surfaces of these particles scatter the incoming laser light and increase the overall intensity counts in the spectra. When the laser is turned off, the source of scattering is removed, and an equivalent drop is seen in the spectra.

The slope of the release does not immediately go to zero, most likely due to the following factors: (1) pores have larger apertures in the *cis* orientation (see Fig. 1), allowing for some residual diffusion of cargo molecules, (2) a delay caused by diffusion of cargo from the MOF particles to the laser detection area is expected, and (3) thermal back-conversion processes continue to generate a small amount of motion in the dark. Most of these effects are expected to be short-lived, however, and discontinuation of laser irradiation is expected to eventually reduce the rate of dye release to a negligible level. Since continuous laser irradiation is needed for efficient expulsion of the dye into solution, the pattern and duration of release can be adjusted as necessary. Azo-IRMOF-74-III, therefore, is useful in applications where longer release or stop-start release is desired.[43–45]

Conclusions

An azobenzene-derivatized MOF has been synthesized and studied spectroscopically. Azobenzene *trans* and *cis* isomerizations of the linker molecule have been observed *via* NMR and absorption spectroscopy to ascertain the relative concentrations and the absorption spectra of the *cis* and *trans* species as well as the most appropriate wavelength choices for irradiation.

Irradiation at 408 nm, near the linker's isosbestic point, causes both *cis–trans* and *trans–cis* excitations. The large amplitude motions due to these wagging motions led to an increase in dye mobility, expelling cargo from the structure on demand. The storage and release capabilities of the system were studied with the aid of fluorescent propidium iodide, and the dye release rate was diminished when irradiation was removed. No release was observed prior to irradiation, indicating that the dye molecules are well contained.

The photo-driven azo-MOF structure, the focal point of this paper, is an improvement over recently made photoswitchable frameworks in that this structure contains only one-dimensional pores. The one-dimensional pores permit more efficient storage and release of the dye, and the microporous particles allow filtration in a new size domain. Here, we have shown that the azo-MOF structure is capable of storing dye molecules and releasing them on command *via* a photoisomerization process. This new MOF creates unprecedented possibilities for the use of light in the realm of robust dynamics.

Acknowledgements

This work was supported by DTRA/US Army Research Office (Grant W911NF-07-1-0533).

Notes and references

1 M. Eddaoudi, D. B. Moler, H. L. Li, B. L. Chen, T. M. Reineke, M. O'Keeffe and O. M. Yaghi, *Acc. Chem. Res.*, 2001, **34**, 319–330.
2 S. L. James, *Chem. Soc. Rev.*, 2003, **32**, 276–288.
3 J. L. C. Rowsell and O. M. Yaghi, *Microporous Mesoporous Mater.*, 2004, **73**, 3–14.
4 H. Deng, S. Grunder, K. D. Cordova, C. Valente, H. Furukawa, M. Hmadeh, F. Gandara, A. C. Whalley, Z. Liu, S. Asahina, H. Kazumori, M. O'Keeffe, O. Terasaki, J. F. Stoddart and O. M. Yaghi, *Science*, 2012, **336**, 1018–1023.
5 B. Chen, L. Wang, Y. Xiao, F. R. Fronczek, M. Xue, Y. Cui and G. Qian, *Angew. Chem., Int. Ed.*, 2009, **48**, 500–503.
6 A. Lan, K. Li, H. Wu, D. H. Olson, T. J. Emge, W. Ki, M. Hong and J. Li, *Angew. Chem., Int. Ed.*, 2009, **121**, 2370–2374.
7 J.-R. Li, R. J. Kuppler and H.-C. Zhou, *Chem. Soc. Rev.*, 2009, **38**, 1477–1504.
8 N. L. Rosi, J. Eckert, M. Eddaoudi, D. T. Vodak, J. Kim, M. O'Keeffe and O. M. Yaghi, *Science*, 2003, **300**, 1127–1129.
9 J. L. C. Rowsell and O. M. Yaghi, *Angew. Chem., Int. Ed.*, 2005, **44**, 4670–4679.
10 C. D. Wu, A. Hu, L. Zhang and W. B. Lin, *J. Am. Chem. Soc.*, 2005, **127**, 8940–8941.
11 D. Farrusseng, S. Aguado and C. Pinel, *Angew. Chem., Int. Ed.*, 2009, **48**, 7502–7513.
12 R. C. Huxford, J. Della Rocca and W. Lin, *Curr. Opin. Chem. Biol.*, 2010, **14**, 262–268.
13 H. M. D. Bandara and S. C. Burdette, *Chem. Soc. Rev.*, 2012, **41**, 1809–1825.
14 K. Hoffmann, U. Resch-Genger and F. Marlow, *Microporous Mesoporous Mater.*, 2000, **41**, 99–105.

15 C. M. Stuart, R. R. Frontiera and R. A. Mathies, *J. Phys. Chem. A*, 2007, **111**, 12072–12080.
16 N. G. Liu, Z. Chen, D. R. Dunphy, Y. B. Jiang, R. A. Assink and C. J. Brinker, *Angew. Chem., Int. Ed.*, 2003, **42**, 1731–1734.
17 W. Freyer, D. Brete, R. Schmidt, C. Gahl, R. Carley and M. J. Weinelt, *J. Photochem. Photobiol., A*, 2009, **204**, 102–109.
18 J. Han, D. Yan, W. Shi, J. Ma, H. Yan, M. Wei, D. G. Evans and X. Duan, *J. Phys. Chem. B*, 2010, **114**, 5678–5685.
19 S. Angelos, E. Choi, F. Vogtle, L. De Cola and J. I. J. Zink, *Phys. Chem. C*, 2007, **111**, 6589–6592.
20 C. Barrett, A. Natansohn and P. Rochon, *Macromolecules*, 1994, **27**, 4781–4786.
21 E. Besson, A. Mehdi, D. A. Lerner, C. Reye and R. J. P. Corriu, *J. Mater. Chem.*, 2005, **15**, 803–809.
22 Y. Einaga, O. Sato, T. Iyoda, A. Fujishima and K. Hashimoto, *J. Am. Chem. Soc.*, 1999, **121**, 3745–3750.
23 E. Johansson, E. Choi, S. Angelos, M. Liong and J. Zink, *J. Sol-Gel Sci. Technol.*, 2008, **46**, 313–322.
24 D. Y. Kim, S. K. Tripathy, L. Li and J. Kumar, *Appl. Phy. Lett.*, 1995, **66**, 1166–1168.
25 G. S. Kumar and D. C. Neckers, *Chem. Rev.*, 1989, **89**, 1915–1925.
26 T. Naito, K. Horie and I. Mita, *Polymer*, 1993, **34**, 4140–4145.
27 M. Ogawa, K. Kuroda and J.-I. Mori, *Chem. Commun.*, 2000, 2441–2442.
28 P. Sierocki, H. Maas, P. Dragut, G. Richardt, F. Vögtle, L. De Cola, F. Brouwer and J. I. Zink, *J. Phys. Chem. B*, 2006, **110**, 24390–24398.
29 S. Yagai, T. Karatsu and A. Kitamura, *Chem.–Eur. J.*, 2005, **11**, 4054–4063.
30 Y. Yang, X. Wang, L. Liu, X. Xie, Z. Yang, R. K. Y. Li and Y.-W. Mai, *J. Phys. Chem. C*, 2007, **111**, 11231–11239.
31 S. Angelos, Y.-W. Yang, N. M. Khashab, J. F. Stoddart and J. I. Zink, *J. Am. Chem. Soc.*, 2009, **131**, 11344–11346.
32 S. Angelos, E. Johansson, J. F. Stoddart and J. I. Zink, *Adv. Funct. Mater.*, 2007, **17**, 2261–2271.
33 H. Sato, R. Matsuda, K. Sugimoto, M. Takata and S. Kitagawa, *Nat. Mater.*, 2010, **9**, 661–666.
34 A. J. Blake, N. R. Champness, T. L. Easun, D. R. Allan, H. Nowell, M. W. George, J. Jia and X. Sun, *Nat. Chem.*, 2010, **2**, 688–694.
35 K. K. Tanabe, C. A. Allen and S. M. Cohen, *Angew. Chem., Int. Ed.*, 2010, **49**, 9730–9733.
36 C. A. Allen and S. M. Cohen, *J. Mater. Chem.*, 2012, **22**, 10188–10194.
37 R. K. Deshpande, G. I. N. Waterhouse, G. B. Jameson and S. G. Telfer, *Chem. Commun.*, 2012, **48**, 1574–1576.
38 A. Modrow, D. Zargarani, R. Herges and N. Stock, *Dalton Trans.*, 2011, **40**, 4217–4222.
39 J. Park, D. Yuan, K. T. Pham, J. Li, A. Yakovenko and H. Zhou, *J. Am. Chem. Soc.*, 2012, **134**, 99–102.
40 S. Angelos, M. Liong, E. Choi and J. I. Zink, *Chem. Eng. J.*, 2008, **137**, 4–13.
41 S. Angelos, E. Choi, F. Vögtle, L. De Cola and J. I. Zink, *J. Phys. Chem. C*, 2007, **111**, 6589–6592.
42 Y. A. Lau, B. L. Henderson, J. Lu, D. P. Ferris, F. Tamanoi and J. I. Zink, *Nanoscale*, 2012, **4**, 3482–3489.
43 L. Sieminska, M. Ferguson, T. Zerda and E. Couch, *J. Sol-Gel Sci. Technol.*, 1997, **8**, 1105–1109.
44 L. Rossi, G. Brandi, G. F. Schiavano, S. Scarfi, E. Millo, G. Damonte, U. Benatti, A. D. Flora and M. Magnani, *AIDS Res. Hum. Retroviruses*, 1999, **15**, 345–353.
45 L. Yang and R. Fassihi, *J. Controlled Release*, 1997, **44**, 135–140.

